MTOC clustering and nuclear division through proper spindle positioning in yeast: a microtubule grow-and-catch model

Saptarshi Chatterjee,[1,*] Subhendu Som,[1,†]
Neha Varshney,[2,‡] Kaustuv Sanyal,[2,§] and Raja Paul[1,¶]

[1] *Indian Association for the Cultivation of Science, Kolkata -700032, India*

[2] *Molecular Mycology Laboratory, Molecular Biology and Genetics Unit, Jawaharlal Nehru Centre for Advanced Scientific Research, Jakkur, Bangalore -560064, India*

Abstract

The mitotic spindle formation in pathogenic budding yeast, *Cryptococcus neoformans*, depends on multitudes of intertwined interactions primarily between kinetochores, microtubules (MT), spindle pole bodies (SPBs) and various molecular motors. Prior to spindle formation microtubule organizing centers (MTOCs), embedded on the outer nuclear envelope (NE), coalesce into a single SPB. We propose a 'grow-and-catch' model, in which cytoplasmic MTs (cMTs) nucleated by MTOCs grow and catch each other, to facilitate MTOC clustering. Our quantitative modeling analysis supported by experiments, for the first time, identifies multiple redundant mechanisms mediated by cMT- cell cortex interactions via dynein and Bim1, act in synchrony for timely clustering of MTOCs. Implementing a similar stochastic model of 'grow-and-catch' kinetochores, here we demonstrate that pre-clustered kinetochores and highly biased MTs are a pre-requisite for timely capture of duplicated kinetochores. Further, in the absence of an error correction mechanism, the mitotic division culminates in a biased and asymmetric distribution of the nuclear mass. The model predicts that either a marginal delay in MT nucleation from the daughter SPB or an enhanced MT nucleation from the mother SPB can independently account for the asymmetry as observed in the experiment.

*Electronic address: sspsc6@iacs.res.in
†Electronic address: sspss5@iacs.res.in
‡Electronic address: nehavarshney@jncasr.ac.in
§Corresponding author: sanyal@jncasr.ac.in
¶Corresponding author: raja.paul@iacs.res.in

Introduction

Spatio-temporal dynamics of organelle-constituents relies primarily on the active organization of microtubules (MTs). Microtubules are semiflexible polymeric filaments having rapidly polymerizing plus ends and slowly polymerizing minus ends with its growth and shrinkage being governed by intrinsic dynamic instability parameters [1]. In animal cells centrosome serves as a major structural template for nucleation of MTs leading to the formation of a radial MT array [2–4]. However, the radial spanning of MTs in many noncentrosomal MT networks is governed by various membrane organelles (e.g. Golgi apparatus) [2, 5–9]. The cellular structures that harbor the ability to nucleate MTs, subsequently gets stabilized followed by the structural organization of a radial network are referred as Microtubule Organizing Centers (MTOCs) [2, 10].

In the budding yeast spindle pole bodies (SPBs), embedded on the NE fill the shoes of a centrosome. The SPBs are enriched with distinct $\gamma-$tub receptors that organize the cytoplasmic and nuclear MTs [11, 12]. In *Saccharomyces cerevisiae* the biochemical machinery controlling the active 'ring shaped' nucleation template for the MTs involves a core building block of γ-tubulin. TUB4 gene encodes γ-tubulin which physically interacts with Spc98, Spc97 to form γ-tubulin small complexes (γ-TuSCs). Subsequently, the receptors of γ-TuSc, Spc110 and Spc72, localize γtubulin complexes to the SPBs and form a γ-tubulin ring complex (γ-TuRC). This provides SPBs distinct nuclear and cytoplasmic domains referring to the fact that a single MTOC can accommodate nucleation sites for both cytoplasmic and nuclear MTs [2, 10, 13].

In contrast to *S. cerevisiae*, where the SPB being the only MTOC, there are several MTOCs present in basidiomycete budding yeast *Cryptococcus neoformans* during interphase [14]. MTOCs embedded on the NE wade along the NE toward each other and fuse together to form the mother SPB (mSPB) eventually when the cell voyages into the mitosis. In *C. neoformans* self-assembly of MTOCs is orchestrated by MT mediated 'grow-and-catch' (also known as 'search and capture') on the NE [14, 15]. The optimized clustering mechanisms are not explicitly organism specific and the basic characteristic underpinnings of the clustering mechanisms are shared across diverse set of organisms as well as several other sets of organelle assemblies (e.g. Golgi assembly and stacking, mitochondrial assembly etc.) [8]. The mechanistic understanding of the MTOC clustering prior to the formation of the mSPB

in *C. neoformans* remains elusive and experimentally challenging, thus calls for an '*in silico*' study to canvass the paradigm.

After the formation of the mSPB marked by SPB activation, the SPB is duplicated and duplicated SPBs separate from each other resulting in the formation of the spindle (biorientation). Each SPB nucleate two sets of microtubules namely, cytoplasmic MTs (cMTs) and nuclear MTs (nMTs). The plus ends of cMTs interact with the cell cortex via a myriad of microtubule-associated proteins (MAPs) and molecular motor proteins. The force transduction via the concerned MTs drives the local movement of the spindle regulating the spindle positioning and migration toward the daughter bud. Proper spindle positioning is not only a prerequisite for equal segregation of the nuclear mass but the placement of the spindle also ascertains the plane of the division [14, 16]. In animal cells, the location of the spindle marks the position where the contractile ring is formed to segregate the daughter cells [17]. Asymmetric positioning of the spindle results in an unequal nuclear segregation amongst the daughter cells. In budding yeast, a particular location where the mitotic division occurs is predetermined even before the formation of the spindle [14, 18]. The spindle positioning within a confined geometry with an underlying spatial symmetry can often be mapped onto a centering problem. For example, force transduction via the active force generators at the cell cortex leads to the centering of the spindle in HeLa cells culminating in a symmetric division with cortical pull being the key contributor in the force balance landscape [19]. Similar spindle localization at the cell center is also observed in *Caenorhabditis elegans* embryo during early prophase [20]. Interestingly, in budding yeast *C neoformans* the spindle is formed within the daughter bud marked by the bilateral separation of SPBs. Henceforth, prior to the spindle formation, the spatiotemporal maintenance of the nucleus SPB conglomerate suggests a directed movement toward the daughter bud from the mother [15, 16]. In *S. cerevisiae*, timely nuclear migration toward the mother-daughter bud neck juncture requires directed force generation toward the daughter bud. This directed movement stems from the interplay between dynein pull on the plus ends of the cMTs at the mother and daughter cortex along with Bim1 mediated bias of the cMTs supported by a MyoV based machinery in the mother bud [16]. Our previous study [15] shows that there is a differential spatial arrangement of dynein puncta across the mother and the daughter cell cortex in *C. neoformans*. In the daughter cell cortex, we observed a single large condensed dynein patch, whereas in the mother cortex dynein puncta are small and distributed. This spatial

organization refers to the fact that net directed pull from the daughter cortex mediated by concentrated dynein molecules in association with Bim1 overrides the opposing pull from the mother cell cortex leading to a net nuclear migration toward the daughter bud. Moreover, the default distributed spatial arrangement of dynein patches in the mother cortex (unlike the highly condensed localized patch in the daughter) further reduces resultant pulling force from the mother cortex. Therefore, the nucleus cruises into the daughter bud under the influence of the directed pull from the daughter cortex. Whether the spindle achieves a stable position following nuclear migration is a crucial determinant of the faithful nuclear segregation. Using a mathematical model in 1-dimension that includes various MT mediated forces originating from the mother and the daughter cell cortex, we explore the spindle stability inside the daughter cortex in presence of MT buckling transition, cortical pull from both mother and daughter cells in harness with instantaneous cortical push on the MTs. Our numerical analysis quantifies the spindle localization away from the mother-daughter bud neck juncture determined by the magnitude of the competing molecular forces sprouting from both the mother and the daughter cortex. Quantitatively, the stability of the spindle position is characterized by stable and unstable fixed points.

The proposition from earlier studies indicates that the interdigitated nMTs crosslinked via kinesins and other molecular players initiate the formation of spindle architecture where some of the nMTs establish contact with all the kinetochores [21, 22]. It is observed that during budding yeast mitosis, the kinetochores remain in a 'preclustered' configuration [14, 23]. An optimized grow-and-catch process results in the formation of stable attachments (amphitelic) linking individual sister kinetochores to opposite SPBs by kinetochore MTs (kMTs) essential for accurate chromosome segregation during cell division [24, 25]. In the 'grow-and-catch' process enacted by the MTs and kinetochores, chromosomes actively establish a contact with the SPBs. The conundrum regarding the 'grow-and-catch' process was first elucidated in terms of a random 'search and capture' process exploiting MT dynamic instability [26]. It has been shown that the efficiency of 'grow-and-catch' relies on the cell shape, initial position of the centrosome and phenomenological observation based fine-tuning of dynamic instability parameters, adaptive changes in spatiotemporal arrangement of kinetochores etc. [27–29]. Taking cues from the earlier studies and our experimental results, we employed a minimalistic computational model to explore the role of MT dynamic instability and spatial MT bias toward kinetochore precluster to attain an 'all kinetochores captured' configuration

within the relevant mitotic time scale. Our model analysis demonstrate that for the efficient capture of all the kinetochores, the 'searcher' MT beam needs to be rendered focused toward the kinetochore precluster. The predictive nature of our '*in silico*' model indicates that the likely plausible mechanisms for the focused MT rendition are default directed nucleation of MTs toward the kinetochore cluster and a chemical gradient dependent modulation of catastrophe frequency around the chromosomes [27].

The timely capturing of all kinetochores leads to four possible configurations of kinetochore-MT attachments [30, 31]. When the sister kinetochores are captured by MTs from opposite SPBs, stable amphitelic attachments are established. When sister kinetochores are linked to the same SPB, erroneous syntelic attachments are established. When one sister kinetochore is attached to the pole but the other sister kinetochore is dangling around being unattached, monotelic attachments are formed. Another plausible configuration is when both the sister kinetochores are unattached. The erroneous non-amphitelic kinetochore-MT attachments lead to various defects like unequal segregation, aneuploidy; the ramifications of which are attributed to cancer [31–33]. This leads to another avenue of conundrum that how the erroneous attachments are progressively rectified to yield a stable 'all-amphitelic' configuration so that equal segregation of nuclear mass during division is achieved. The amphitelic attachments are achieved by two central mechanisms. First, the error-correction mechanism that detects and destabilizes the incorrect kinetochore-MT attachments, thereby giving cells another chance to achieve biorientation. Second, the Spindle assembly checkpoint (SAC) process that senses the attachment state of the kinetochores and delays the anaphase onset until amphitely is achieved. Previous studies report that the error-correction mechanism in budding yeast is governed by the Aurora B kinase homologue Ipl1 where erroneous kinetochore-MT attachments (e.g. low tension syntelic attachments) are degraded via Ipl1 mediated phosphorylation of individual kinetochore proteins. The high-tension bioriented amphitelic attachments do not fall under the purview of Ipl1 governed phosphorylation cloud and remain stabilized [31, 34–38]. Our study indicates that in absence of error correction mechanism in *C. neoformans*, a skewed distribution of segregated mother daughter nuclear volume may arise where the daughter cell lacks the euploid nuclear content [15]. Our computational analysis together with experimental observations further alludes that the origin of this skewness can be traced back to the differential maturation of the SPBs [39]. In this study, using a computational model we propose plausible mechanisms

either acting alone or in liaison in order to illustrate how the mother bud retains more nuclear mass than the daughter bud. Either a delay in MT nucleation from the SPB going to the daughter bud or nucleation of more MTs from the SPB in the mother bud compared to the SPB in the daughter bud would suffice in replicating the experimentally observed template of unequal segregation.

Results

Clustering of MTOCs progresses via a myriad of redundant pathways

Previously, we demonstrated that several MTOCs embedded over the outer NE uniformly are required to conglomerate into a compact mass to form the fully functional mother SPB in *C. neoformans* prior to spindle formation [15]. However, the mechano-transduction pathways for the MTOC clustering leading to the formation of a SPB are yet to be elucidated. Therefore, we explored various plausible MT driven mechanisms that facilitate MTOC clustering in the *'in silico'* model (Figure 1A). In the *in silico model*, we assume that MTOCs colocalize with kinetochores (Cse4) [40, 41] and MTOC clustering indirectly regulates the process of kinetochore clustering. Since the kinetochores and MTOCs are linked together, prior to the formation of the mother SPB, we looked into the temporal evolution of kinetochore clustering as an indirect yardstick to estimate the time required for MTOC clustering in *C. neoformans*. The average experimental timescale for kinetochore clustering is ~ 25 min (Figure 1B).

First, we tested the possibility that the cMTs growing out of the MTOCs and grazing along the NE can directly grow and catch the MTOCs. In the model, a distinct subset of MTs emanating from the MTOCs are confined to the NE and subsequently graze along the NE with the 'searcher' MT tips remaining close to the embedding surface (NE). When the tip of a grazing MT ('searcher') nucleated from a MTOC encounters another MTOC ('target') along its trajectory and establishes a contact, they start to wade toward each other along the NE until they fuse together (Figure 1A). For simplicity we assumed that two MTOCs 'linked' by a grazing MT, are 'blind' to MT mediated interactions from other MTOCs until their fusion. We found that the timescale for complete clustering achieved by this 'direct grow-and-catch' pathway is significantly large surpassing all the relevant timescales involved

in the mitosis. It is unlikely to be an 'efficient' pathway for MTOC clustering and thus not considered further to be the sole pathway. However, the possibility that the same pathway may work in combination with other more efficient pathways cannot be ruled out.

Previous studies showed that [14, 15, 42–44] the cortical interaction of the cMTs (MT-cell cortex interaction) mediated by numerous motor proteins transduce directed mechanical forces on various intracellular components. Henceforth, we investigated whether the dynein mediated MT- cell cortex interaction plays a pivotal role in this process. In this mechanistic template, we considered cMTs emanating from the MTOCs, trudge through the cytoplasm and reach the cell cortex. Subsequently, cortical dyneins anchor into the MT segments sliding in the inner layer of the cell cortex. The force generated due to dynein activity imparted on the cMTs inside the cell cortex is, however, transmitted via the concerned MTs to the MTOCs resulting in a constrained mobilization of MTOCs embedded on the NE. The MTOCs fuse together upon contact with each other. We found that the exclusive activity of dynein mediated MT- cell cortex interaction leads to nearly complete clustering of the MTOCs (Figure 1C) but the required time estimated ($\sim$ 240 min) exceeded the experimentally observed time range of $\sim$ 25 min (Figure 1B). Within the experimental time window of $\sim$ 25 min only partial clustering ($\sim$ 45 %) is attained exclusively via MT-cell cortex interaction (Figure 1D). This result provided us with evidence that MT-cortex interaction alone does not generate adequate force to complete the clustering of all MTOCs and form a mature SPB within $\sim$ 25 min (Figure 1B).

Unrealistic clustering time predicted by these mechanisms prompted us to consider alternative pathways for timely clustering of the MTOCs. Apart from cMTs searching for the MTOC, we introduced interaction among grazing cMTs on the NE via dynein crossbridging (inter cMT coupling at the NE) (Figure 1A). A considerable number of cMTs interact on the NE due to crosslinking activity of dynein motors acting at the MT-MT overlap [45] (Figure 1A). Inward sliding of the overlapping cMTs from two different MTOCs steered by dynein motors facilitate rapid fusion of the engaged MTOCs. We found that 'inter cMT coupling at the NE' along with MT- cell cortex interaction culminated in a complete clustering ($\sim$ 99 %) of the MTOCs within $\sim$ 25 min (Figure 1C,1D). Moreover, the clustering solely via 'inter cMT coupling at the NE' alone can accomplish the fusion of all the MTOCs ($\sim$ 100 %) within $\sim$ 23 min (Figure 1C, 1D).

Cellular processes involving MT mediated 'grow-and-catch' mechanisms, are often opti-

mized by the regulation of the number of MTs [46, 47]. In a similar 'search and capture' process, as the MT number increases, the capture time gradually plummets down to a threshold timescale followed by a saturation [48]; the scenario implies that upon step wise increase in the number of MTs per MTOC, the clustering time is expected to decrease (Figure 1E). The observations from our computational model reveal that an optimized set of MTs is essential for MTOC clustering occurring within the experimental time window. We explored a number of possibilities where the MT number per MTOC is kept constant upon clustering of two MTOCs, adding the MT number upon fusion of the MTOCs up to a maximum limit to 4 MTs per MTOC and then removing the maximum limit respectively (Figure 1E).

Force generation on the MTOCs via nuclear interaction is primarily regulated by the collective activity of dyneins engaged at the MT-MT overlap. Net force generated by the dyneins at the overlap facilitates sliding of anti-parallel MTs, which in turn brings over concerned MTOCs closer to each other. Higher the dynein force per MT at the overlap on the NE, faster the MTOCs merge with each other via 'inter cMT coupling at the NE' (Figure 1F). Apart from these, MT-cortex interaction with Bim1 mediated bias (MT-cortex interaction with bias) can be a potential mechanism for timely clustering due to the effective drift applied on the MTOCs [15].

Together, these results reveal that the clustering time accomplished by the 'inter cMT coupling at the NE coupled with MT- cell cortex interaction' and 'inter cMT coupling at the NE' alone corroborate with the experimentally measured time scale reasonably well (Figure 1B, 1C, 1D). The clustering mechanisms involving MT-cortex interaction with bias [15], inter cMT coupling at the NE collaborated with MT- cell cortex interaction and sole activity of inter cMT coupling at the NE are redundant and are employed in the model system in such a way that they either could work in liaison or could accomplish the job alone. This indicates that these schemes are not strictly necessary to be functional in a parallel manner during the self-organization of MTOCs. If one mechanism is absent or fails, the other one will act as a backup mechanism to facilitate the process of clustering. Further, in view of uncertainty in the number of kinetochores associated with a single MTOC, we explored the asynchronous assembly of kinetochores and MTOCs. Our model predicted that proper kinetochore clustering within the experimental period is feasible even if more than one kinetochore is attached to a single MTOC (Figure 1G).

In the current study, upon monitoring the model observations we conclude that there is a

prevalence of redundancy amongst the diverse set of MT-driven mechanisms for MTOC clustering (Figure 1C). It was evident that the MTOCs have to wend along the NE collectively toward each other until they coalesce to form a single mature SPB.

The complete clustering of MTOCs marks the formation of the mature mother SPB followed by the duplication to give rise to two daughter SPBs. Consequently, the duplication of SPBs is followed by separation of SPBs into a configuration that initiates spindle formation. From literature and our earlier study, comprising experiment and coarse-grained simulation ([15]), it has been shown that the mitotic spindle stabilizes inside the daughter bud at a location close to the septin ring in *C. neoformans*. These observations prompted us to build up a mathematical description accounting for the dynamic force balance landscape within the cell that governs the spindle localization (See Materials and Methods, Supplementary Information, Figure S1). We subsequently analyze the role of various MT mediated forces in fostering the proper spindle positioning case by case, both individual force contributions as well as while acting in tandem (Figure 2A-2I).

Spindle positioning can be determined from the balance of mechanical forces in the cell

A spindle is constantly acted upon by molecular forces arising from the interactions of its components with the surrounding [14, 15], e.g., cMTs interacting with the cell cortex via dynein generates a pull on the nucleus toward the cell periphery; similarly, cMTs buckling in contact with the cell membrane pushes the nucleus away from the membrane. These interactions are plausible in both mother and daughter cell cortex. In addition, interactions of cMTs with the septin ring and the cortical actin cables generate an effective bias translating the plus ends of the cMTs toward the daughter bud. Since these forces are spatially inhomogeneous and rapidly varying with time, it is logical to ask how the nucleus and the spindle attain steady positions prior to the chromosomal segregation.

We formulate an analytical template in one dimension that accommodates all key MT-mediated force contributors originating from the mother and daughter cortex acting on the SPBs (Figure S1). The mechanistic force balance landscape arising out of the default mathematical template allows us to carry out sensitivity analysis across a wide parameter regime constituting a myriad of forces with different mechanobiological characteristics (e.g. instan-

taneous pushing and buckling of the cMTs, dynein mediated pulling etc.). From experiments and agent based simulation, we observe that the average spindle length is around ~ 1.5 μm in wild-type (Figure S2A) and the neck to spindle distance is close to ~ 1 μm while the spindle is in the daughter bud (Figure S2B). Also the spindle lies almost parallel to the axis of symmetry (orientation angle ~ 15 deg) joining the centers of mother-daughter bud (Figure S2C).

In the following, we discuss about the analytical findings illustrating the combined effects of various forces on the spatial maintenance of a bilaterally symmetric spindle within the mother or daughter bud (See Supplementary Information for details). Our analysis reveals that the competition solely amongst the instantaneous pushing forces on the SPBs from the mother and daughter cell cortex stably position the spindle inside the mother bud (Figure 2A) whereas the tug of war between the dynein mediated cortical pull from the mother and daughter cortex introduces unstable spindle positions (Figure 2B). The unstable spindle positions certify that a small fluctuation in the mechanical force balance leads to a complete collapse of the spindle either on the mother cortex or on the daughter cortex. In other words, if the spindle is positioned at any of the unstable fixed points, a small force perturbation on the spindle in the direction of mother (daughter) cortex would lead to a stable localization of the spindle on the mother (daughter) cortex. Interestingly, the presence of a cortical pull in harness with the instantaneous cortical push leads to a stable transition of the spindle from the mother (daughter) to the daughter (mother) cell cortex via a string of unstable spindle positions as the cortical dynein density is varied (Figure 2C-2E). Variation in the average MT length also plays a critical role in spindle positioning (Figure 2F). It is imperative to note here that the experiments suggest a stable spindle position close to the septin ring inside the daughter bud. The analytical prescription, however, reveals that the competing interplay between instantaneous cortical push and dynein mediated cortical pull is insufficient for the stable spindle localization close to the septin ring inside the daughter bud. Further investigation reveals, force transduction due to MT buckling in both the mother cell cortex and the daughter cell cortex is crucial for proper spindle positioning. The sensitivity analysis based on our theoretical model predicts that the balance among the forces acting on the spindle dominated by MT buckling renders stable spindle positions close to the septin ring inside the daughter bud (Figure 2G-2I). Further, upon considering differential spatial arrangement of dyneins in mother and daughter cortex (as observed in previous

experiments [15]), the sensitivity analysis found a myriad of mechanistically relevant force balance landscapes crafted with stable as well as unstable positions of the spindle (Figure S2D-S2F).

Efficient chromosomal capture prior to SPB biorientation requires bias in MT searching

During early stages of spindle formation, nMTs randomly grow and catch kinetochores. Initially, MTs form monotelic (one of the sister kinetochores attached to MT) attachments with the kinetochores that eventually transform into syntelic (both the sister kinetochores are attached to MTs from the same SPB) or amphitelic (sister kinetochores are correctly attached to MTs from opposite SPBs) attachments. Merotelic attachment (the sister kinetochores attached to same SPB) does not occur due to a single MT binding site at the kinetochore. Implementation of the stochastic 'grow-and-catch' kinetochores via nuclear MTs revealed that timely capture of all the kinetochores would require a pre-clustering of the kinetochores and highly biased/focused MTs toward the cluster (Figure 3). We explored several MT-mediated 'grow-and-catch' mechanisms facilitating the encounter of kinetochores with 'Searcher' MT tips marked by the large scale MT length fluctuation originating from the intrinsic dynamic instability. Since the *C. neoformans* undergoes a semi-open mitosis, only the nuclear MTs emanating from the SPBs 'sniff' out the kinetochores. To investigate the role of MTs in timely chromosomal capture within a confined geometry (nucleus, r_{nuc}= 1.0 μm), we first simulated MTs with fixed dynamic instability parameters scanning the entire nuclear volume without any spatial preference. We found that with the increase in the number of 'searcher' nMTs, the net kinetochore ('target') capture time decreases quite consistently (Figure 3A and S3A). In addition, the capture time depends upon the location of the kinetochore cluster. The initial kinetochore-MT encounter (nMT=24) with the kinetochore cluster localized at the nuclear center takes $\sim$ 10 min for complete capture of all the kinetochores whereas it plummets down to $\sim$ 3 min when the kinetochore cluster is localized halfway in between the SPBs and the nuclear center. Upon significant decrease in nMT number (nMT=14), $\sim$ 70 % of the kinetochores remain unattached even after $\sim$ 50 min which exceeds relevant mitotic time scales observed from experiments. Thus, the mechanism without any spatially biased nMTs is inefficient in ensuring timely capture of all

the kinetochores for a wide range of physiological parameters.

We further investigated the possibility of a biased MT-nucleation toward the preclustered kinetochores. In this mechanism, MTs nucleate from the SPBs remain constrained within a solid angle toward the kinetochore cluster (Figure 3B and S3B). We hypothesize that the MT nucleation sites on the SPBs might be designed in such a manner that the entire nMT population is rendered 'focused'/ biased toward the kinetochore cluster. Our computational analysis reveals that the biased MT nucleation leads to the capture of entire kinetochore population within $\sim$ 2 min (nMT=24) when the kinetochore cluster is positioned halfway in between the SPBs and the nuclear center and within $\sim$ 5 min (nMT=24) when the kinetochore precluster is at the nuclear center (Figure S3B and 3B). Even upon statistically significant decrease in the MT number (nMT=14), $\sim$ 80 % kinetochores establish MT attachment within $\sim$ 30 min which alludes to the robustness and enhanced efficiency compared to the unbiased mechanism.

Next, we looked into the spatial dependence of MT's stability on the absolute concentration of a chemical cue synthesized at the kinetochore and how this influences the timely capture (See Supplementary Information for details). Computational model implementing this mechanism suggests inefficient capture similar to Figure 3A & S3A (Figure S3C). Next, we tested the role of the chemical concentration gradient, instead of the absolute concentration. It is evident from Figure 3C and S3D that the timescale for the complete chromosomal capture closely mimics the scenario with 'biased MT nucleation' over a significant variation in the number of MTs. However, when the number of nMT is 14, only $\sim$ 50 % chromosomes are captured via a gradient dependent search in the explored parameter space in contrast to the $\sim$ 80 % capture via 'biased MT-nucleation' (Figure 3C and 3B). This suggests that the mechanism accounting for the 'biased MT-nucleation' is relatively more efficient compared to the concentration gradient dependent search within the explored parameter regime.

Stochastic MT-kinetochore attachment with impaired error-correction leads to aneuploidy and unequal nuclear segregation

Lifetime of a MT-kinetochore attachment is closely linked with the interkinetochore distance and presence of checkpoint protein kinase. Low tension kinetochore-MT attachments, such as syntelic and monotelic attachments undergo degradation owing to the phosphoryla-

tion of kinetochore proteins whereas high tension amphitelic attachments are bioriented and stabilized [31]. In the high tension amphitelic attachments, the bioriented configurations are stretched to the extent that their destabilization is ruled out. The low tension non-amphitelic attachments on the other hand undergo destabilization as their poorly stretched geometric configurations fall under the influence of phosphorylation gradient of the checkpoint protein preventing aneuploidy. Incorporating this notion in our computational model, we quantified the aneuploidy in normal and Ipl1 depleted *C. neoformans* cells as shown in Figure 4A- 4K. Erroneous attachments occurring due to the random events of MT 'grow-and-catch' kinetochores are corrected following degradation of the wrong attachments (Figure 4A, S4A, S4B). Our model predicted that a higher degradation rate of wrong attachments resulted in a faster attainment of a stable amphitelic configuration (Figure 4B).

Our experimental observations indicate that the SPBs mature differentially in mother and daughter buds of the wild-type *C. neoformans* cells. The SPB which matures faster (the brighter SPB) goes to the daughter bud in most of the cases in wild-type (Figure 4C-4D). However, other possibilities also exist in minority of the cells. In the analysis, the SPB closer to the mother bud was considered as mSPB (mother SPB) and the other one was considered as the dSPB (daughter SPB). However, the eventual fate of the two SPBs in terms of stable spatial localization inside the mother bud or the daughter bud cannot be exactly ascertained from the current experimental setup. We assumed that the SPB closer to the mother bud will eventually come back to mother cell and the SPB which is away from the mother bud will be retained in the daughter bud without the re-orientation the spindle. In contrary to the wild-type scenario, the difference in intensity of the SPBs is not distinguishable in the Ipl1 depleted cells (Figure 4C-4D). These observations indirectly refer to the possibility of asymmetric functionality between the two SPBs, in the early stages of spindle formation.

In view of the fact that the size distribution of the mSPB and dSPB are different, we hypothesize that the average number kinetochore-MT attachments from the mSPB and the dSPB might differ. The apparent difference in the attachments made by the mSPB and dSPB might also be manifested via a delay in MT nucleation from the mSPB or the dSPB. However, upon Ipl1 depletion, segregated mother daughter nuclear volume ratio tends to shift toward > 1 unlike the wild-type scenario where we observe equal nuclear division [15]. Note that *in silico* description of the nuclear content volume is assumed to be proportional to the number of sister chromatids. The shift of the ratio toward > 1 upon Ipl1 depletion reflects

that the total nuclear volume within the mother is higher than that within the daughter. In the present model construction, this is rendered feasible only when there is a delay in nMT nucleation from the dSPB. More specifically, the delay in nMT nucleation from the dSPB enhances the number of syntelic attachments from the mSPB. The phenomenological basis of the delay lies in the fact that the mother bud retains a greater amount of nuclear mass due to an unequal sharing of erroneous attachments by the mSPB and the dSPB. Interestingly in wild-type cells, since a correction mechanism is present, the initial syntelic attachments made from the mSPB eventually degrade and amphitelic configurations emerge, resulting in an equal segregation of the nuclear mass. However, in Ipl1 depleted cells, since error correction mechanism is compromised, the syntelic attachments from the mSPB survive. From Figure 4E and 4F, it is evident that as the delay in MT nucleation from the dSPB increases, the segregated mother-daughter nuclear volume ratio increases accordingly.

Our computational model also indicates an alternate plausible mechanism that may account for the greater nuclear mass retained by the mother bud in absence of the error correction. During early spindle assembly, the number of kinetochore-MT attachments established by a SPB is proportional to the number of nMTs emanating from the SPB. If the number of nMTs emanating from the SPB inherited by the mother bud (mSPB) is greater than the other SPB (dSPB) that eventually settles inside the daughter bud, it is likely that the mSPB will capture more kinetochores compared to the dSPB promoting an enhanced syntelic attachments attributed to the mother bud. In the wild-type scenario since the correction mechanism is functional, the syntelic attachments formed by the mSPB will be degraded as the time progresses. The steady state configuration will culminate in an error-free all amphitelic template resulting in an equal segregation of nuclear mass between the mother and the daughter bud (Figure 4H). In absence of the aforesaid correction mechanism, the sister kinetochores in a syntelic configuration lack the ability to cut all ties with the attached MTs. Henceforth comparatively greater number of erroneous attachments from the mSPB are maintained all throughout resulting in aneuploidy followed by the skewness in the distribution of segregated mother daughter nuclear mass ratio (Figure 4I). In a nutshell, enhanced syntelic attachments formed by the mSPB are resolved in wild-type achieving an equal segregation of the nuclear mass. The equal segregation is consistent across the variation in the number of nMTs emanating from the dSPB while the number of nMTs from the mSPB is kept constant at 24. In the absence of error correction mechanism the enhanced

syntelic attachments amassed by the mSPB do not undergo degradation contributing to the heightened nuclear volume in the mother bud. Interestingly, as the nMT number from the dSPB gradually approaches the number of MT from mSPB (24), the ratio moves toward unity and the error accumulated by each of them also equalize.

In view of the emerging defects in MTOC clustering and nuclear migration in Ipl1 depleted cells, we also canvassed the possibility where the kinetochores are captured from multiple MTOCs prior to the SPB maturation. More specifically, in a configuration where MTOC clustering is delayed, we posit that even after the formation and duplication of the SPBs, some partially clustered MT nucleating fragments may take long time to fuse with the larger cluster committed to form the SPBs. This simply stems from the fact that in presence of shorter MTs owing to their compromised intrinsic structural integrity in Ipl1 depleted condition, complete fusion of all the MTOCs is hindered [15]. Hence, it is possible that the SPB maturation is promoted even when a few unclustered MTOCs are left out. If those 'left out' MTOC fragments participate in kinetochore capture via a parallel 'grow-and-catch' mechanism, followed by a delayed fusion, chances of an unequal division becomes prominent in the absence of error correction mechanism (Figure S4C). In order to accommodate the phenomenological observation of higher DNA volume retained by the mother bud, 'left out' MTOC fragments are allowed to merge with the SPB in the mother bud. This predictive model template alludes that higher the number of MTs in the fragmented MTOCs, more nuclear volume will be retained by the mother bud yielding a > 1 mother daughter nuclear volume ratio (Figure S4C).

Since Ipl1 has been shown to monitor erroneous kinetochore-MT attachments to prevent chromosome mis-segregation in Ascomycota [31, 34, 35, 49], we previously estimated the fidelity of chromosome segregation during mitosis in Ipl1-depleted cells in *C. neoformans* as a representative species of the phylum Basidiomycota [15]. The computational model predicted nuclear volume-fraction in a post-anaphase scenario appeared to correlate with the experimental data [15] both in wild type scenario and in ipl1 depleted cells assuming delayed MT nucleation from the daughter SPB (Figure 4J-4K).

Discussion

In this study, constructing a coarse-grained mechanistic model, together with microscopic observations, we show that the timely clustering of MTOCs in reasonable synchrony with kinetochore clustering orchestrates the proper formation of the mSPB followed by SPB duplication, nuclear migration and subsequent development of the spindle architecture leading to faithful, high fidelity chromosomal segregation. Our computational analysis reveals that the clustering of MTOCs is primarily a MT mediated phenomenon, where force generation by dynein, Bim1 and other motors at cell cortex and NE transduced via the interacting MTs leads to locally directed mobilization of MTOCs constrained on the NE. Subsequently, coalescence of multiple MTOCs into a single compact mass forms the mSPB. Our model identifies three relatively independent pathways, functioning via the MT- cell cortex interaction with biased MT plus end gliding along the cortex [15], MT-MT interaction with direct search for the MTOCs along the NE and MT- cell cortex interaction coupled with MT-MT interaction along the NE, lead to timely clustering. The outcome further indicates a possible redundancy amongst these mechanisms while acting in concert (Figure 1A-1G).

In the experiments, it is observed that the spindle architecture in *C. neoformans* passages into the daughter bud, but remains near the bud neck juncture marked by the septin ring during the metaphase. Also the plane of mitotic division is defined by this stable positioning of the spindle apparatus inside the daughter bud [50] having the orientation of the spindle almost parallel to the axis connecting the centers of the mother and daughter buds[14, 15]. These findings prompted us to build up a minimalistic 1-dimensional analytical model to explore the sensitivity of various force balance landscapes that evaluates the stable positioning of the spindle. Our analysis uncovers that in absence of MT buckling transition, an interplay between instantaneous cortical push and dynein mediated pull leads to a string of stable and unstable fixed points of the spindle position as the dynein density in mother and/or daughter cortex and average MT length are varied gradually. The unstable spindle positions always appear to be sandwiched between a pair of stable positions. Thus, the spindle sitting at an unstable position can migrate into the nearby stable positions depending upon the magnitude and direction of a perturbation (2D, 2E, 2F). In absence of MT buckling transition, the interplay among the other governing forces, namely instantaneous pushing and dynein mediated pulling, fails to render a stable contour of the spindle position

inside the daughter bud close to the septin ring. In fact, in this context the stable contours are found to be localized at the cortex (Figure 2B-2F). When force transduction due to MT buckling acts in harness with dynein mediated pull and instantaneous push from both the mother and the daughter cortex, stable spindle positions appear in the vicinity of the bud neck juncture inside the daughter bud (Figure 2H) indicating the functional importance of MT buckling in maintaining the proper spindle positioning. The presented mathematical model can be extended to higher dimensions in future studies. The default model setup in the higher dimensions will allow us to include several important characteristic degrees of freedom (e.g. angular displacement of the SPBs, torque on the spindle etc.) in the numerical analysis as well.

Directional bias in MT searching is a prerequisite for timely capture of the chromosomes prior to SPB biorientation. The '*in silico*' structural template is a minimal coarse grained spindle architecture within a realistic cellular confinement (Figure 3A-3D and Figure S3A-S3D), where the nMTs explore the nuclear volume and 'sniff' out kinetochores preclustered within. Since the SPBs remain close by right after the duplication, all the kinetochores gets uniformly exposed to both the SPBs. This leads to an initial attachment statistics of ~ 50 % amphitelic and 50 % syntelic, once all the kinetochores are captured. Our study further reveals that there might be at least two parallel pathways that can lead to the timely capture: (a) nucleation of the MTs from the SPBs may be biased toward the kinetochore precluster due to specific organization of the nucleation sites. Accordingly, the MTs do not explore the complete nuclear volume. In fact in fission it has been observed that nMTs explore a section of the constrained nuclear volume via pivoted diffusion while searching for the kinetochores [51–53]. (b) The presence of a RanGTP like chemical gradient may prevent MTs undergoing premature catastrophe and stabilize them as they grow toward the kinetochore cluster. Previous computational and experimental studies illustrated the evidence of a similar gradient dependent MT stabilization rendering a higher MT density 'cloud' around the chromosomes [29, 47, 54]. In the present context, we theoretically articulated that the gradient-based MT stabilization furnishes a focused beam of 'searcher' MTs yielding a timely capture within the explored parameter space. We further showed that the gradient-based mechanism, rather than the absolute concentration, works in favor of the timely capture of the kinetochore cluster.

Our theoretical model further demonstrates that an unattached kinetochore captured

by nuclear MTs via an optimized 'grow-and-catch process' results in the formation of either a low-tension syntelic attachment or a stable high-tension amphitelic attachment. The low-tension syntelic attachments are degraded to the monotelic attachment under the influence of Ipl1-mediated phosphorylation gradient. In the absence of phosphorylation gradient, abundant stable syntelic attachments are established in Ipl1 depleted cells [34, 35]. Nevertheless, in the current model, in the absence of the correction mechanism, the total numbers of erroneous attachments are equally shared by both the SPBs. However, the experimental observations clearly reveal that the nuclear division is unequal and the mother-daughter nuclear volume ratio is > 1 evincing a relatively greater nuclear mass content in the mother cell [15]. To account for the unequal segregation in the model output, an additional delay is introduced in MT nucleation from the daughter SPB. Regardless of the place where the pre-existing SPB or the duplicated progeny SPB eventually settles down, previous studies exhibit a significant delay in the maturation of one of the two SPBs [55, 56]. A delayed MT nucleation from the daughter SPB shifts the segregated mother-daughter nuclear mass ratio to a higher value (> 1) in the cell population that lacks the ability to rectify erroneous attachments [15]. In order to trace back the origin of the skewness in absence of error correction, we explored another likely mechanism where MT distribution in the SPBs is asymmetric. Previous reports demonstrate that in cultured vertebrate cells, the centrosome inherited by the mother possesses more astral MTs compared to the daughter centrosome [57, 58]. More specifically, the mSPB nucleates more nMTs than the dSPB. We observed that in presence of a highly focused beam of nMTs showering onto the kinetochore precluster, the mSPB accumulates more syntelic attachments, eventually yielding a skewed distribution with mean segregated mother daughter nuclear mass ratio > 1. Reports discussing about multicentrosomal clustering suggest that as the centrosomes cluster into two fully operational spindle poles serving the bipolar spindle template, the 'left out' unclustered centrosomes are rendered inactive for proper progression into mitosis. The inactive 'stray' centrosomes contain relatively less amount of $\gamma-$tubulin (impaired MT nucleation) compared to the operational spindle poles [59, 60]. In our *in silico* template, we also explored a plausible paradigm where even after the SPB maturation and duplication, there is a presence of 'active' 'stray' fragmented MTOCs nucleating MTs and participating in kinetochore capture. Subsequently, if the fragmented MTOCs merge with the matured SPB retained by the mother bud, the latter would contain higher amount of nuclear volume compared to the daughter progeny in

absence of the Ipl1 mediated correction (Figure S4C). Taken together, we posit that Ipl1 ensures high-fidelity chromosome segregation via monitoring the kinetochore-MT attachments (Figure 4E-4F).

Materials and Methods

Construction of a strain expressing triple GFP epitope-tagged SPC98 under the native promoter in the wild-type

To monitor the dynamics of MTOCs or SPBs during cell cycle, we constructed the strain expressing Spc98 tagged with triple GFP under the native promoter (CNNV117). The $5'$ coding region of the SPC98 ORF was amplified from genomic DNA of H99 using oligos NV478 and NV479, and cloned into ClaI and KpnI sites of the plasmid pCI3GFPN that contained the triple GFP epitope and NEO resistance gene, to construct pCS3GFPN. The $3'$ untranslated region (UTR) of the SPC98 ORF was amplified from genomic DNA of H99 using oligos NV477 and NV476, and cloned into the SacI site of pCS3GFPN to obtain pCS3GFPNDS. The obtained plasmid was used as a template to amplify SPC98-3xGFP cassette using oligos, NV478 and NV477 and introduced into H99 using biolistic transformation to obtain CNNV117.

Media and growth conditions

The conditional mutant strains IPL1 under the control of the GAL7 promoter were grown in YPG (1 % yeast extract, 2 % peptone, 2 % galactose) as a permissive medium and YPD (1 % yeast extract, 2 % peptone, 2 % dextrose) as a non-permissive medium. The deletion mutant strains were grown in YPD. All the C. neoformans strains were grown at 30° C.

Microscopic image acquisition and processing

The conditional mutant strains were grown till OD600=1 in the permissive medium and re-inoculated in the non-permissive media for 8 h. The deletion mutant strains were grown in YPD overnight. These cells were pelleted at 4,000 rpm and washed once with 1x phosphate buffered saline (PBS). The cell suspension was placed on a thin growth medium containing

2 % agarose patch present on the slide which was covered by a coverslip. The images were acquired at room temperature using laser scanning inverted confocal microscope LSM 880-Airyscan (ZEISS, Plan Apochromat 63x, NA oil 1.4) equipped with highly sensitive photo-detectors or Axio Observer Calibri (ZEISS). The Z- stack images were taken at every 0.5 μm and processed using ZEISS Zen software/ImageJ. All the images were digitally altered with minimal adjustments to levels and linear contrast till the signals were highlighted. Similarly, live-cell imaging was performed at 30° C on an inverted confocal microscope (ZEISS, LSM-880) equipped with a temperature-control chamber (Pecon incubator, XL multi SL), a Plan Apochromat 100x NA oil 1.4 objective and GaAsp photodetectors. Two-color images were taken by the sequential switching between RFP and GFP filter lines (GFP/FITC 488, mCherry 561 for excitation and GFP/FITC 500/550 band-pass, mCherry 565/650 long-pass for emission). For time-lapse microscopy of mCherry-CENP-A and GFP-Tub1, images were collected at a 2-min interval with 1.5 % intensity exposure and a 60-s interval with 1 % intensity exposure respectively, with 0.5 μm Z-steps. All the images were displayed after the maximum intensity projection of images at each time using ImageJ.

Post-acquisition analysis

The intensities of Spc98-3X GFP signals were quantified using a circle tool in ImageJ. The intensities were measured after the 2D rendering of Z-images with ImageJ. The mean integrated densities were quantified for the two poles and were subtracted by the background. The nuclear volumes were obtained as discussed previously ([15]) and these values were used to calculate nuclear volume ratio of the mother versus daughter cell.

Simulation Procedure

Modelling the cellular confinement

The nucleus is taken as a sphere of radius r_{nuc}. The geometric construction that represents the whole cell is considered to be an instantaneous intersection of two unequal spheres of radius R_M and r_d. The septin ring is marked by the circle spanned at the intersection of the two spheres representing the mother and the daughter bud. The mother bud volume remain constant, while the growth rate of the daughter bud is tuned taking cue from the

experimental observations. Underneath the cell boundary, a cortical layer of finite width l_c accounts for the MT interaction at the cortex. The characteristic parameters (e.g. dynein density etc.) of the cortical layer at the mother bud and at the daughter bud are controlled independently due to possible functional differences at the molecular level [14, 15].

Modelling the MTs

The MTs are modelled as semiflexible polymers characterized by four innate dynamic instability parameters, viz, growth velocity (v_g), shrinkage velocity (v_s), catastrophe frequency (f_c) and rescue frequency (f_r). While probing for an alternative mechanism, f_c of the MTs searching for the kinetochores is modulated by the local chemical concentration/concentration gradient. MTs hitting the cortex experience dynein pull, undergo buckling transition when pivoted and apply an instantaneous pushing force. A subpopulation of MTs, graze along the cortex and the NE .

Modelling MTOCs and kinetochores

The kinetochores and MTOCs are modelled in a similar fashion as done in the previous studies [14, 15]. MTOCs are rigid spheres embedded on the NE and the movement of the MTOCs are strictly confined to the outer layer of NE only.

Similarly kinetochores are also modeled as rigid spheres with a hard-core repulsion deployed to prevent any finite overlap amongst the kinetochores. The repulsive force is proportional to the instantaneous overlap between two overlapping kinetochores [15]. A couplet of sister kinetochores remains paired with each other by the cohesin spring until metaphase. A Hookean force proportional to the inter-kinetochore separation is introduced amongst the sister kinetochores to account for the effect of cohesin spring holding them together [14, 15]. The parameters relevant for the development of the computational model are chosen from the previous studies [14, 15].

Spindle positioning in budding yeast: A mathematical prescription in one dimension

In 2-dimensions we consider that the mother and the daughter bud constitute two intersecting circles of radii R_M and r_D respectively. The axis of symmetry of the cellular confinement (e.g. the mother-daughter conglomerate) is taken to be the X-axis with the origin 'O' being set at the center of the mother bud. The center of the daughter bud is placed at a distance 'd' from the center of the mother (Figure S1). We compute various MT based forces on the spindle upon MT interaction with the cell cortex. The mathematical formulation of various force balance terms (e.g forces originating from MT pushing, dynein mediated pull on the MTs at the cell cortex, MT buckling etc.) is characterized by exponential length distribution of MTs [22, 42]. For details, see the Supplementary Information.

Acknowledgments

We acknowledge the help of P. Iyer in the image acquisition and image analysis of nuclear volumes using Imaris 7.6.4 software at ACTREC. This work was supported by the fellowship from SERB (Science and Engineering Research Board), Department of Science and Technology (DST), India (EMR/2017/001346) to RP and Tata Innovation Fellowship (BT/HRD/35/01/03/2017) to KS. SC was supported by fellowship from the University Grants Commission (UGC), India, SS was supported by the fellowship from INSPIRE (IF131156) program DST, India, and NV was supported by the fellowship (09/733 (0253)/219-EMR-I) from Council of Scientific & Industrial Research (CSIR), India.

[1] M. Dogterom and S. Leibler, Physical Review Letters **70(9)**, 1347 (1993).

[2] J. Wu and A. Akhmanova, Annu. Rev. Cell Dev. Biol. **33**, 4.14.25 (2017).

[3] M. Bornens, Science **335**, 42226 (2012).

[4] P. T. Conduit, A. Wainman, and J. W. Raff, Nat. Rev. Mol. Cell Biol. **16**, 611 (2015).

[5] V. Rodionov, E. Nadezhdina, and G. Borisy, PNAS **96**, 11520 (1999).

[6] K. Chabin-Brion, J. Marceiller, F. Perez, C. Settegrana, A. Drechou, G. Durand, and C. Poüs, Mol. Biol. Cell **12**, 204760 (2001).

[7] L. Hurtado, C. Caballero, M. P. Gavilan, J. Cardenas, M. Bornens, and R. M. Rios, Journal of Cell Biology **193**, 91733 (2011).

[8] T. Vinogradova, R. Paul, A. D. Grimaldi, J. Loncarek, P. M. Miller, D. Yampolsky, V. Magidson, A. Khodjakov, A. Mogilner, and I. Kaverina, Mol. Biol. Cell **23**, 82033 (2012).

[9] T. Vinogradova, P. M. Miller, and I. Kaverina, Cell Cycle **8**, 2168 (2009).

[10] J. Paz and J. Lüders, Trends in Cell Biology **28(3)**, 176 (2018).

[11] J. V. Kilmartin, Philos Trans R Soc Lond B Biol Sci. **369**, 20130456 (2014).

[12] T. chen Lin, A. Neuner, and E. Schiebel, Trends Cell Biol. **25**, 296307 (2014).

[13] T. chen Lin, A. Neuner, Y. T. Schlosser, A. N. Scharf, L. Weber, and E. Schiebel, Elife **3**, e02208 (2014).

[14] S. Sutradhar, V. Yadav, S. Sridhar, L. Sreekumar, D. Bhattacharyya, S. K. Ghosh, R. Paul, and K. Sanyal, Molecular Biology of the Cell **26**, 3954 (2015).

[15] N. Varshney, S. Som, S. Chatterjee, S. Sridhar, D. Bhattacharyya, R. Paul, and K. Sanyal, PLoS Genet **15(2)**, e1007959 (2019).

[16] F. J. McNally, J. Cell Biol. **200(2)**, 131 (2013).

[17] R. A. Green, E. Paluch, and K. Oegema, Annu. Rev. Cell Dev. Biol. **28**, 29 (2012).

[18] C. G. Rasmussen, J. A. Humphries, and L. G. Smith, Annual Review of Plant Biology **62**, 387 (2011).

[19] T. Kiyomitsu and I. M. Cheeseman, Nat. Cell Biol. **14**, 311 (2012).

[20] D. H. Park and L. S.Rose, Dev. Biol. **315**, 42 (2008).

[21] M. Winey and K. Bloom, Genetics **190(4)**, 11971224 (2012).

[22] N. P. Ferenz, R. Paul, C. Fagerstrom, A. Mogilner, and P. Wadsworth, Curr Biol. **19(21)**,

18331838 (2009).

[23] M. Anderson, J. Haase, E. Yeh, and K. Bloom, Mol Biol Cell **20**, 4131 (2009).

[24] C. E. Walczak, S. Cai, and A. Khodjakov, Nat Rev Mol Cell Biol. **11(2)**, 91 (2010).

[25] R. Heald and A. Khodjakov, J. Cell Biol. **211(6)**, 1103 (2015).

[26] M. Kirschner and T. Mitchison, Cell **45**, 329 (1986).

[27] R. Paul, R. Wollman, W. T. Silkworth, I. K. Nardi, D. Cimini, and A. Mogilner, PNAS **106(37)**, 15708 15713 (2009).

[28] V. Magidson, C. B. O. Connell, J. Lončarek, R. Paul, A. Mogilner, and A. Khodjakov, Cell **146**, 555 (2011).

[29] V. Magidson, R. Paul, N. Yang, J. G. Ault, C. B. OConnell, I. Tikhonenko, B. F. McEwen, A. Mogilner, and A. Khodjakov, Nature Cell Biology **17**, 11341144 (2015).

[30] M. Winey, C. L. Mamay, E. T. O'Toole, D. N. Mastronarde, T. H. Giddings, K. L. McDonald, and J. R. McIntosh, The Journal of Cell Biology **129(6)**, 1601 (1995).

[31] E. S. Tubman, S. Biggins, and D. J. Odde, Cell Systems **4**, 645 (2017).

[32] G. J. P. L. Kops, B. A. A. Weaver, and D. W. Cleveland, Nature Reviews Cancer **5**, 773785 (2005).

[33] H. Rajagopalan and C. Lengauer, Nature **432**, 338 (2004).

[34] S. Biggins and A. W. Murray, Genes Dev. **15(23)**, 3118 (2001).

[35] S. Biggins, F. F. Severin, N. Bhalla, I. Sassoon, A. A. Hyman, and A. W. Murray, Genes Dev. **13**, 532 (1999).

[36] I. M.Cheeseman, S. Anderson, M. Jwa, E. M.Green, J. Kang, J. R.Yates, C. S.M.Chan, D. G. Drubin, and G. Barnes, Cell **111(2)**, 163 (2002).

[37] H. Dewar, K. Tanaka, K. Nasmyth, and T. U. Tanaka, Nature **428**, 93 (2004).

[38] T. U.Tanaka, N. Rachidi, C. Janke, G. Pereira, M. Galova, E. Schiebel, M. J.R.Stark, and K. Nasmyth, Cell **108(3)**, 317 (2002).

[39] G. Pereira, T. U.Tanaka, K. Nasmyth, and E. Schiebel, The EMBO Journal **20(22)**, 6359 (2001).

[40] V. Yadav and K. Sanyal, mSphere **3(4)**, e00190 (2018).

[41] L. Kozubowski, V. Yadav, G. Chatterjee, S. Sridhar, M. Yamaguchi, S. Kawamoto, I. Bose, J. Heitman, and K. Sanyal, mBio **4(5)**, 00614 (2013).

[42] S. Som, S. Chatterjee, and R. Paul, Phys. Rev. E **99**, 012409 (2019).

[43] S. M. Huisman and M. Segal, Journal of Cell Science **118**, 463 (2005).

[44] J. L. Carminati and T. Stearns, The Journal of Cell Biology **138(3)**, 629 (1997).

[45] M. E. Tanenbaum, R. D. Vale, and R. J. McKenney, eLife , 2:e00943 (2013).

[46] Z. Bertalan, Z. Budrikis, C. A. M. L. Porta, and S. Zapperi, PLOS ONE , 10.1371/journal.pone.0141305 (2015).

[47] R. Wollman, E. Cytrynbaum, J. Jones, T. Meyer, J. Scholey, and A. Mogilner, Current Biology **15**, 828832 (2005).

[48] A. Sarkar, H. Rieger, and R. Paul, Biophysical Journal **116**, 20792091 (2019).

[49] N. Varshney and K. Sanyal, Molecular Microbiology **0(0)**, 1 (2019).

[50] M. K. Balasubramanian, E. Bi, and M. Glotzer, Current Biology **14**, R806R818 (2004).

[51] I. Kalinina, A. Nandi, P. Delivani, M. R. Chacón, A. H. Klemm, D. Ramunno-Johnson, A. Krull, B. Lindner, N. Pavin, and I. M. Tolić-Nørrelykke, Nat Cell Biol. **15(1)**, 82 (2013).

[52] A. R. Lamson, C. J. Edelmaier, M. A. Glaser, and M. D. Betterton, Biophysical Journal **116**, 1719 (2019).

[53] I. Nayak, D. Das, and A. Nandi, bioRxiv , http://dx.doi.org/10.1101/673723 (2019).

[54] D. J. Odde, Current Biology **15(9)**, R328 (2005).

[55] S. L. Shaw, E. Yeh, P. Maddox, E. D. Salmon, and K. Bloom, J Cell Biol. **139(4)**, 985994 (1997).

[56] D. A. Lerit, J. T. Smyth, and N. M. Rusan, Chromosome Res. **21(3)**, 271286 (2013).

[57] M. Piel, P. Meyer, A. Khodjakov, C. L. Rieder, and M. Bornens, J Cell Biol. **149(2)**, 317 (2000).

[58] Y. M. Yamashita, A. P. Mahowald, J. R. Perlin, and M. T. Fuller, SCIENCE **315**, 518 (2007).

[59] R. Basto, K. Brunk, T. Vinadogrova, N. Peel, A. Franz, A. Khodjakov, and J. W. Raff, Cell **133**, 10321042 (2008).

[60] A. Kramer, B. Maier, and J. Bartek, Molecular Oncology **5(4)**, 324 (2011).

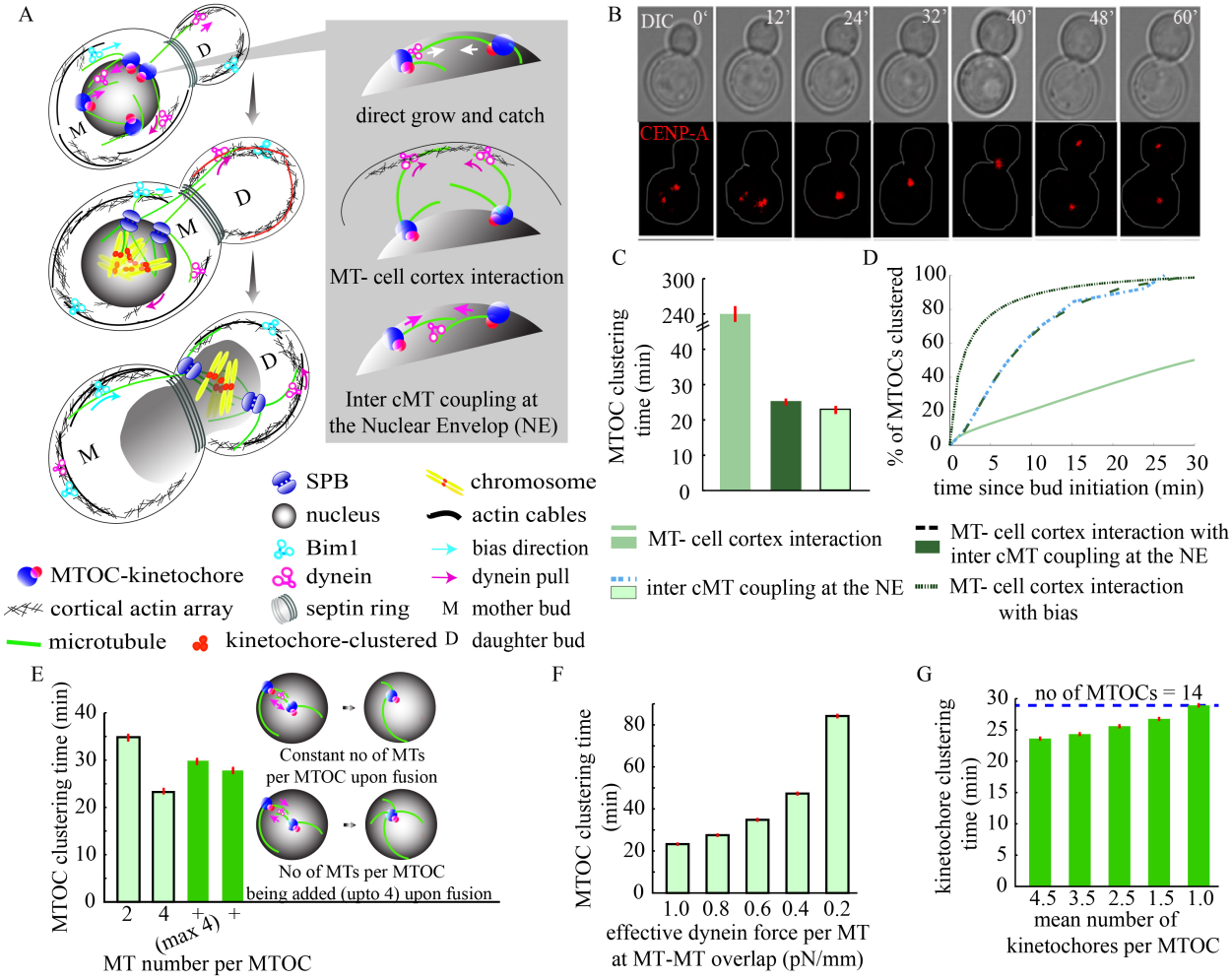

Figure 1. Cooperative interactions among cortical and cytosolic determinants lead to an optimized MTOC clustering and nuclear migration. (A) Schematic of MTOC clustering, nuclear migration, biorientation of chromosomes and possible chromosomal attachments. Arrows indicate direction of forces. A growing cMT directly catching an MTOC ('direct grow-and-catch'), or cMT plus-ends interacting with cortical dyneins (MT-cortex interaction) or sliding of anti-parallel cMTs via crosslinking dyneins on the nuclear surface (inter cMT coupling at the NE) can independently lead to MTOC clustering. (B) Time-lapse snapshots of the wild-type CNVY107 cells expressing inner kinetochore marker mCherry-Cse4 at the indicated time. Bar 5 μm (C) Mean MTOC clustering time since the bud emergence for various MT mediated pathways (n $\geq$ 31). (D) Percentages of MTOC clustered due to various mechanisms. (E) (First and second bar graphs from left) MTOC clustering time having constant number of cMTs per MTOC, i.e. upon fusion, the number of cMTs emanating from the fused MTOC remains the same as that of the individual fusing

MTOCs. Clustering solely via 'inter cMT coupling at the NE' is deployed here. (Third bar) MTOC clustering time when every MTOC nucleates single cMT at the onset of the simulation and upon fusion the MT pools from the fusing MTOCs aggregate up to a maximum of 4 cMTs per MTOC. (Fourth bar) Similar to the "Third bar" but no constraint on the maximum number of cMTs per MTOC. (F) MTOC clustering time in sole presence of inter cMT coupling at the NE via dynein mediated crosslinking the MT-MT overlap. The clustering time (obtained via inter CMT coupling at the NE) increases as the effective dynein force per MT at the MT-MT overlap decreases. The MT number per MTOC is kept constant as 4 all throughout. (G) Asynchronous assembly of kinetochores/MTOCs, if more than one kinetochore is associated with a single MTOC. In all figures, sample size n>2000 for simulation and red bars indicate SEM.

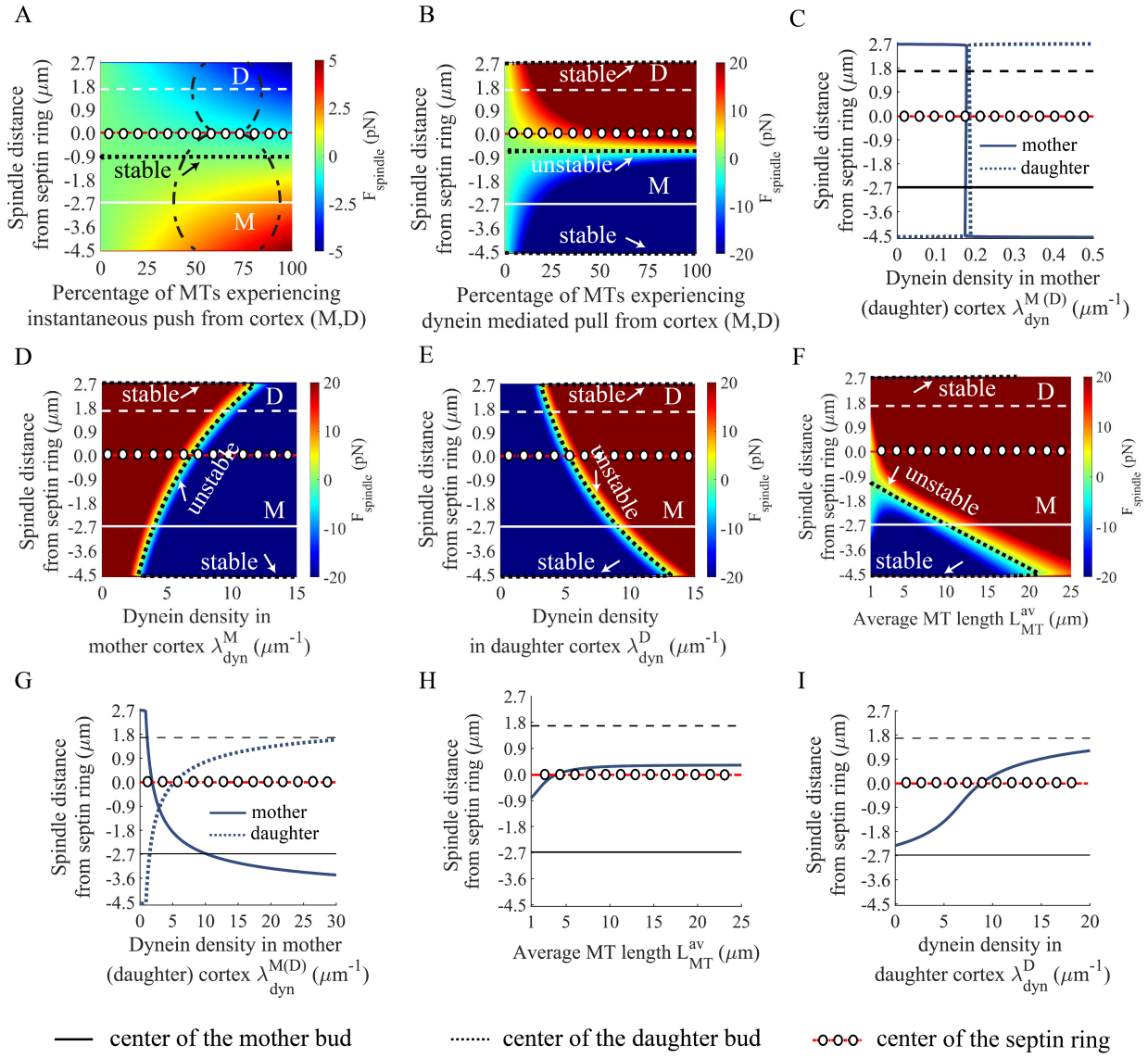

Figure 2. A mechanistic force balance template illustrates the spindle positioning within a budding yeast cell. In all the figures, -ve/+ve distance refers to the spindle in mother (M)/daughter (D) bud. The white dashed and solid lines denote center of the daughter and mother bud respectively, in the color map plots. Colorbars represent the net force on the spindle (A) In the sole presence of instantaneous MT-mediated cortical push from mother and daughter cortex, the spindle stabilizes (dotted black line) close to the septin ring inside the mother cortex. (B) Sole activity of dynein mediated cortical pull from the mother and daughter cortex via cytoplasmic MTs leads to three fixed positions for the spindle: two stable fixed positions are at the mother and the daughter cortex respectively and one unstable fixed position (dotted black line) located near the septin ring inside the

mother bud. (C) Variation in dynein density in the mother (daughter) cortex ($\lambda_{dyn}^{M(D)}$) facilitates a spatial transition in the spindle localization when instantaneous cortical push and dynein mediated pull from the mother (daughter) act simultaneously. The spatial transition is designated by a sharp changeover in stable spindle positioning from mother (daughter) to daughter (mother) cortex. (D-E) Position of the spindle subject to the variation in the dynein density in the mother (daughter) cortex ($\lambda_{dyn}^{M(D)}$) with fixed dynein density in the daughter (mother) cortex when instantaneous cortical push and dynein mediated pull work together from the mother and daughter cortex. Upon step wise increase in dynein density ($\lambda_{dyn}^{M(D)}$), a gradual changeover in spindle positioning occur via a slew of unstable spindle positions marked by the 'Z' and 'inverted Z' contours (black dotted lines) respectively. (F) Variation in average MT length (L_{MT}^{av}) in absence of MT buckling leads to a string of unstable spindle positions sandwiched between stable position-contours at the mother and the daughter cortex when instantaneous cortical push and dynein pull act in tandem. (G) Increase in dynein density in the mother (daughter) cortex ($\lambda_{dyn}^{M(D)}$) results in a rapid changeover in spindle localization from the daughter (mother) to the mother (daughter) bud when instantaneous push, dynein pull and MT buckling in the mother (daughter) cortex act together. Force due to MT buckling dominates in spindle close to the mother (daughter) cortex. (H) Variation in average MT length (L_{MT}^{av}) in presence of instantaneous cortical push, dynein pull and MT buckling at both mother and daughter cortex affirms stable spindle positioning in the vicinity of the septin ring within the daughter cortex. (I) Upon stepwise increase in dynein density in the daughter cortex (λ_{dyn}^{D}), the spindle gradually moves into the daughter cortex, stably localizing near the septin ring.

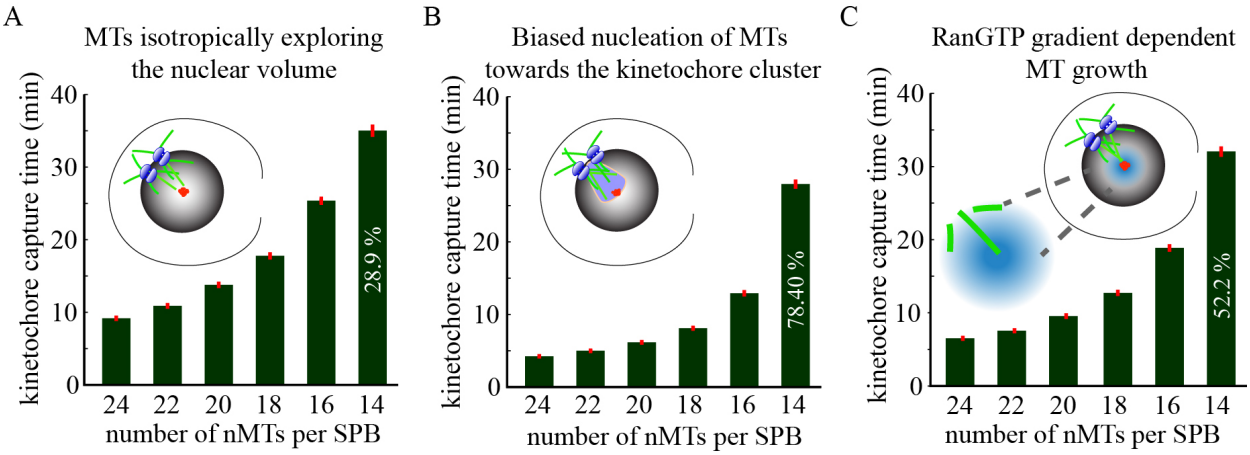

Figure 3. Kinetochore capture facilitated by 'searching' nuclear microtubules (nMT) indicates a plausible template accommodating spatial bias for efficient capture. (A) Capture time of the kinetochore cluster located at the center of the nucleus (schematic in inset) upon variation in the number of nMTs with all the nMTs exploring the nuclear volume isotropically in an unbiased manner. (B) Capture time of the kinetochore cluster upon variation in the number of nMTs when the MT nucleation is biased toward the kinetochore cluster as shown in the inset schematic. (C) Kinetochore capture-time upon variation in the number of nMTs when the direction of MT growth is modulated by the local concentration gradient of RanGTP like molecules. Higher the concentration gradient of RanGTP around the MT plus end, lower the chance of the MT undergoing catastrophe.

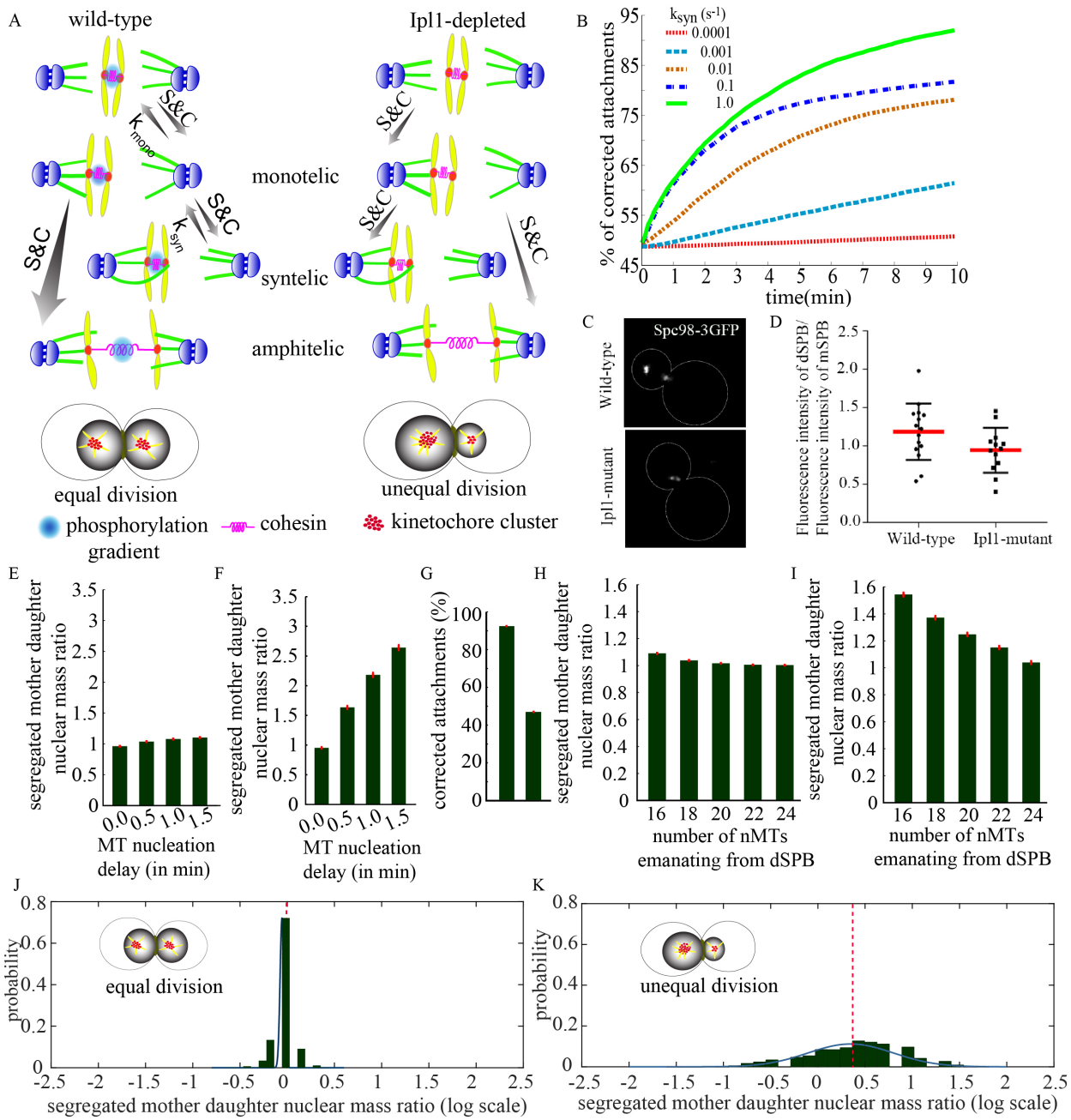

Figure 4. Emergence of aneuploidy in absence of error correction mechanism. (A) Schematic of possible kinetochore-MT attachments and corresponding DNA segregation patterns. (left panel) Stable amphitelic configurations correlate with moiety segregation of DNA volume in wild-type, whereas (right panel) erroneous attachments (syntelic, monotelic) correlate with unequal segregation. (B) Dynamics of error correction is correlated with syntelic degradation rate (k_{syn}). (C) Distribution of Spindle pole body protein, Spc98 during spindle assembly in the wild-type and Ipl1-depleted cells. Microscopic analysis of the distri-

bution of Spindle pole body protein, Spc98-3GFP between mother and daughter buds in the wild-type and Ipl1-depleted cells. (D) Quantification of the ratio of fluorescence intensities of dSPB versus mSPB in the wild-type and Ipl1-depleted cells. (E-F) The delay in MT nucleation from the dSPB does not perturb the equal division when the error correction mechanism is deployed in wild-type cells. In contrast to the wild-type scenario, the MT nucleation delay increases the abundance of erroneous attachments leading to a higher mother to daughter DNA volume ratio in the cell population with no error correction mechanism in place. (G) Attachment statistics in presence of correction mechanism (left bar), and in absence of correction mechanism with $\sim$ 30s delay in MT nucleation from the daughter SPB (right bar). (H-I) Segregated mother daughter nuclear mass ratio upon variation in the number of nMTs nucleating from dSPB in wild-type and in absence of error correction mechanism. The number of nMTs from the mSPB is kept constant at 24. (J-K) Distribution of the ratio of the DNA volume of the mother versus daughter (segregated DNA volumes) in the wild-type and Ipl1 mutant in semi-log scale (the average DNA volume fraction is shown in the inset).